

# Pool boiling heat transfer on double extended surface with mini- and microchannels

Robert Pastuszko<sup>1,2\*</sup>, Robert Kaniowski<sup>1,2</sup>, Norbert Dadas<sup>1,2</sup>, Hubert Danielewski<sup>1</sup>, Krystian Mulczyk<sup>1</sup> and Petra Dancova<sup>3</sup>

<sup>1</sup>Kielce University of Technology, al. Tysiaclecia Panstwa Polskiego 7, PL-25-314 Kielce, Poland

<sup>2</sup>Central Office of Measures, ul. Elekoralna 2, 00-139 Warsaw, Poland

<sup>3</sup>Teplárna Liberec, a.s.. Dr. Milady Horákové 641/34a 460 01 Liberec, Czech Republic

**Abstract.** The paper presents preliminary experimental studies on the effect of additional microchannels made on the extended surface with minichannels on the intensification of heat transfer during nucleate pool boiling. The initial experiments were carried out with saturated water and ethanol. The measurements were performed with increasing heat flux using a double-extended MMC surface (minichannels + microchannels) and a base surface with minichannels (MC). The parallel minichannels (MC) manufactured by machining were 0.5 – 1.1 mm wide and 5.5 to 6 mm deep. The additional microchannels at the top of the fin and at the bottom of the minichannel were 0.15 mm wide and deep. For microchannels texturing the SPI nanosecond single mode pulse laser was used with maximum output power equal to 20 W at wavelength in range 1059 - 1065 nm. The tested MMC surface enabled the achievement of significant heat transfer coefficients: nearly 315 kW/m<sup>2</sup>K for water and over 70 kW/m<sup>2</sup>K for ethanol boiling. For water boiling in the range of 600 to 1150 kW/m<sup>2</sup>, heat transfer coefficients greater than 250 kW/m<sup>2</sup>K were achieved. Approximately 1/3 higher heat transfer coefficients were obtained for the tested double-extended surface (MMC) compared to the most effective minichannel surface (MC), using water and ethanol as working fluids.

## 1 Introduction

The paper involves experimental and theoretical studies of structural surfaces for highly effective heat transfer based on the phase change of the working fluid.

With advances in electronics, nuclear, space, and military technologies, the accommodation of very high-density heat fluxes has become one of the most critical issues. The intensification of heat transfer is also extremely important from an economic and ecological perspective. Nucleate boiling heat transfer has been applied in many types of energy conversion system, e.g. in refrigeration and air conditioning, cooling devices in electric car batteries, high-power electronic systems, avionic components, etc. The highest heat flux at a small temperature difference between the heating surface and the working fluid and a small heat removal surface can be obtained through a phase change accompanying the boiling and condensation processes. Pool boiling on specially prepared surfaces helps to obtain an additional increase in the heat transfer coefficient (HTC), which, in relation to the heat exchanger, translates into higher values of the overall heat transfer coefficient. The increase in the boiling heat transfer coefficient can be attained through passive methods (e.g., extended surfaces in form of mini- and microfins, higher surface roughness, porous covering, mini- and microchannels, subsurface structures or complex systems) or active methods (e.g., providing surface vibration, liquid mixing, spraying and atomization, electric field).

New enhanced surfaces are being extensively studied in many research centers. Kandlikar [1] and Emery et al. [2] classified enhancement techniques into a few main groups:

- increased surface area – fins, minifins, microfins, minichannels, microchannels (Table 1) – boiling of working fluids with low HTC could be enhanced by providing greater surface area and greater nucleation site density;
- increased nucleation – roughness, porous surface, reentrant cavities – heat transfer increases due to the large number of nucleation sites, and the onset of nucleate boiling (ONB) occurs at lower heat fluxes;
- increased evaporation – tunnel-pore structures, meshes [3], foams, micro- and nanostructures – the heat transfer rate is enhanced by increasing the surface area in contact with the liquid film, the wicking structure increases evaporation from curved interfaces over the wicks;
- surface wettability control – mixed wettability, hierarchical micro- and nanostructures – critical heat flux (CHF) increases with decreasing the contact angle, the capillary material provided additional liquid to the base of growing bubble and delayed the dry spot formation;
- separate liquid-vapor flow through bubble-induced macroconvection – departing bubbles inducing an inverted liquid flow over the nonboiling regions;
- other techniques – electric field, surfactant additives, nanofluids, vapor venting, etc.

\* Corresponding author: [tmprp@tu.kielce.pl](mailto:tmprp@tu.kielce.pl)

**Table 1.** Types of open microchannels for pool boiling enhanced heat transfer.

Reference	Configuration	Liquid	The highest HTC
Cooke and Kandlikar [4]	silicon microchannels 40 – 200 $\mu\text{m}$ wide and 180 – 275 $\mu\text{m}$ deep, etched in silicon plates	water	73 $\text{kW}/\text{m}^2\text{K}$
Cooke and Kandlikar [5]	copper microchannels 0.2 – 0.4 mm wide and 0.1 – 0.4 mm deep	water	269 $\text{kW}/\text{m}^2\text{K}$ (channel width 0.375 mm, depth 0.4 mm)
Patil and Kandlikar [6]	microchannels (300—762 $\mu\text{m}$ wide, 200—400 $\mu\text{m}$ deep) with micro-porous coatings on the fin tops	water	995 $\text{kW}/\text{m}^2\text{K}$ for the 762 $\mu\text{m}$ wide channel
Kalani and Kandlikar [7]	copper microchannels 245 – 470 $\mu\text{m}$ deep and 194 – 406 $\mu\text{m}$ wide	ethanol	72 $\text{kW}/\text{m}^2\text{K}$ for 0.207 mm wide and 0.456 mm deep channel
Jaikumar and Kandlikar [8]	copper 762 $\mu\text{m}$ wide and 400 $\mu\text{m}$ deep open microchannel with coating	water	565 $\text{kW}/\text{m}^2\text{K}$
Gheitaghy et al. [9]	copper surface in 45-degree inclined microchannels (widths: 0.5—0.7 mm, depths: 0.5—1 mm)	water	about 120 $\text{kW}/\text{m}^2\text{K}$ (channel width 0.5 mm, depth 1.4 mm)
Kaniowski and Pastuszko [10]	copper microchannels 0.2—0.5 mm deep, 0.2—0.4 mm wide	water	about 392 $\text{kW}/\text{m}^2\text{K}$ (channel width 0.2 mm, depth 0.5 mm)
Hożejwska et al. [11]	copper microchannels 0.2—0.5 mm deep, 0.2—0.4 mm wide	ethanol	about 57 $\text{kW}/\text{m}^2\text{K}$ (channel width 0.2 mm, depth 0.5 mm)
Kalani and Kandlikar [12]	copper open microchannels (widths: 194—406 $\mu\text{m}$ , depths: 245—470 $\mu\text{m}$ ), 16.7—101.3 kPa	ethanol	about 65 $\text{kW}/\text{m}^2\text{K}$ (channel width 0.2, depth 0.456 mm (101.3 kPa))
Rahman and McCarthy [13]	copper microchannel (characteristic length 300 $\mu\text{m}$ to 3 mm) with nanostructured coatings	water	461 $\text{kW}/\text{m}^2\text{K}$
Kwak et al. [14]	copper microchannel with $\text{SiO}_2$ layer (widths: 30 $\mu\text{m}$ , depths: 10—100 $\mu\text{m}$ )	water	about 60 $\text{kW}/\text{m}^2\text{K}$ for the channel width 30 $\mu\text{m}$ , depths 100 $\mu\text{m}$
Walunj and Sathyabhama [15]	rectangular, parabolic, and stepped microchannels with 10-mm diameter copper rod; channel widths: 250—800 $\mu\text{m}$ ; depth: 500 $\mu\text{m}$ .	water	about 16 $\text{kW}/\text{m}^2\text{K}$

## 2 Research methodology

### 2.1 Object of study

Original studies are planned to be carried out to plot the boiling curves and perform visualisation on two types of structure (Figs. 1–3):

- deep minichannels – MC
- minichannels with additional microchannels on the minichannel bottoms and minifin tops – MMC.

The parallel minichannels (MC) manufactured by machining were 0.5 – 1.1 mm wide and 5.5 to 6 mm deep. The additional microchannels at the top of the minifins and at the bottom of the minichannels were 0.15 mm wide and deep (Table 2). For microchannels texturing the SPI nanosecond single-mode pulse laser was used with maximum output power equal to 20 W at wavelength in range 1059 - 1065 nm. In [16] pulsed fiber laser was used to generate longitudinal grooves in the sample.

### 2.2 Experimental setup

The experimental setup proposed in the study is presented in Figures 4 and 5.

### 2.3 Scope of the study

Two working fluids were used in the experiments:

- (1) distilled water ( $T_{sat} \approx 100^\circ\text{C}$ ,  $h_{fg} = 2251 \text{ kJ/kg}$ ),
- (2) ethyl alcohol,  $\text{C}_2\text{H}_6\text{O}$  min. 99.8 % ( $T_{sat} \approx 78^\circ\text{C}$ ,  $h_{fg} = 963 \text{ kJ/kg}$ ).

Three boiling regions were taken into account: onset of nucleate boiling, fully developed nucleate boiling, and boiling crisis.

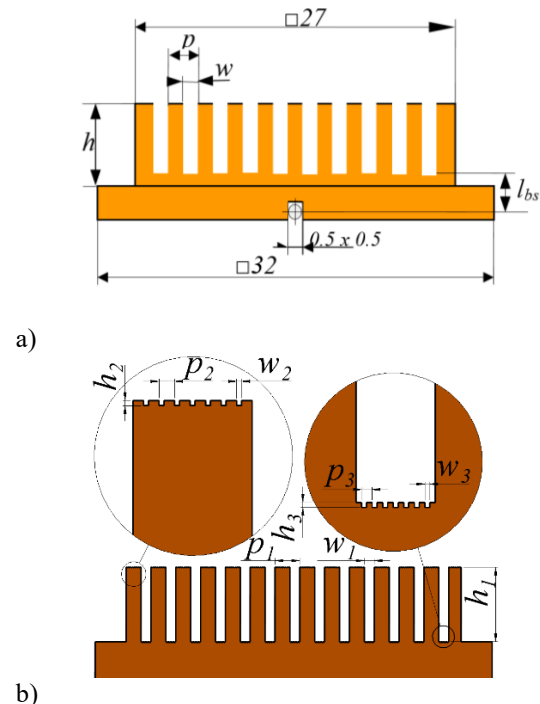


**Fig. 1.** Cross section of the specimens and designation of dimensions. a) MC, b) MMC.

**Table 2.** Surface codes.

Specimen code	$w_1/w_2/w_3$ mm	$h_1/h_2/h_3$ mm	$p_1/p_2/p_3$ mm
MC-0.5-5.5-2	0.5/0/0	5.5/0/0	2/0/0
MC-0.8-6.0-2	0.8/0/0	6/0/0	2/0/0
MC-1.1-5.5-2	1.1/0/0	5.5/0/0	2/0/0
MMC-0.8-6.0-2	0.8/0.15/0.15	6/0.15/0.15	2/0.3/0.3

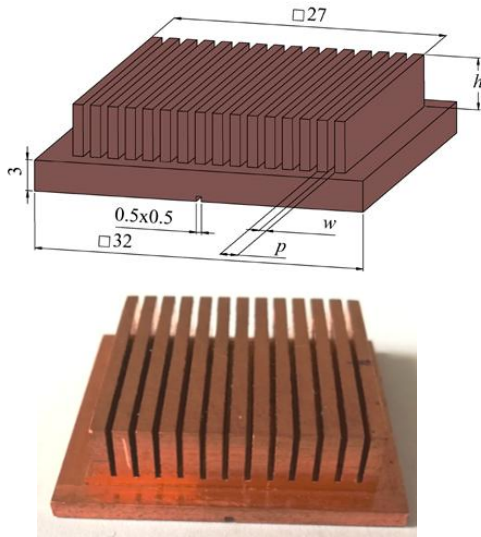


**Fig. 2.** Example of a minichannel surface (MC) planned to be used.

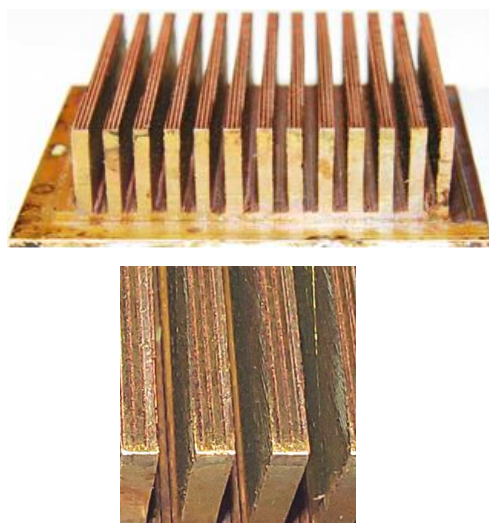
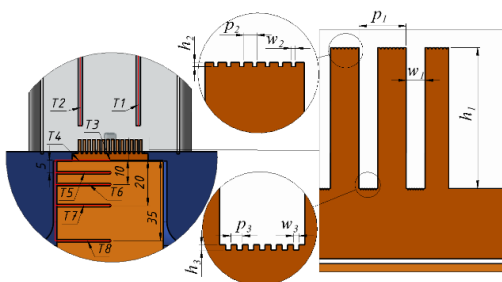


**Fig. 3.** Example of an MMC surface with an enlarged fragment of the minichannel.

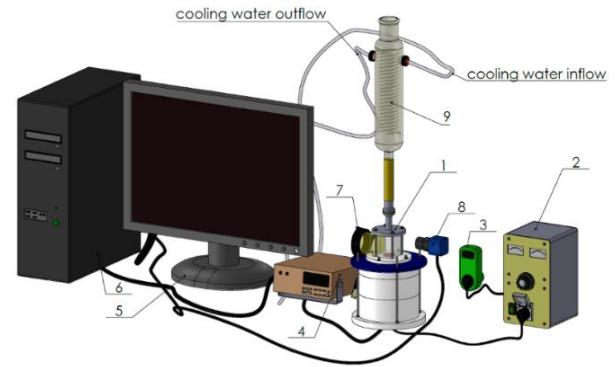


**Fig. 4.** Measurement system: 1 – main module, 2 – autotransformer, 3 – wattmeter, 4 – data logger, 5 – monitor, 6 – PC, 7 – light, 8 – high speed camera/digital camera, 9 – condenser.

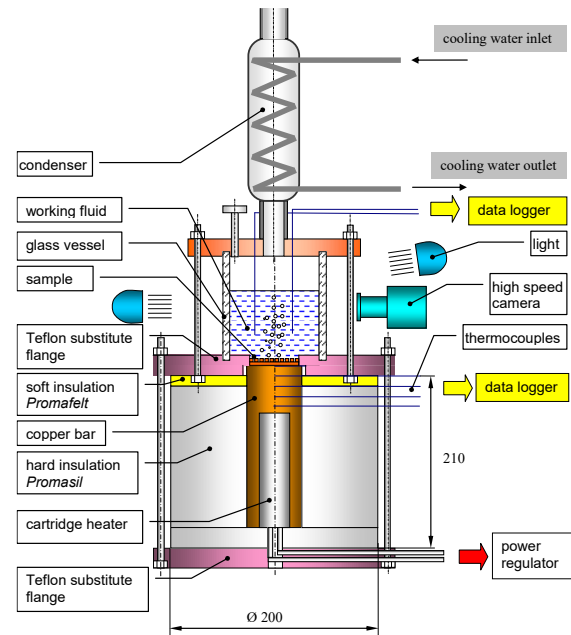


**Fig. 5.** The elements of the main module.

## 2.4 Data reduction

The arrangement of thermocouples is shown in Figure 6. Eight *K*-type thermocouples (NiCr-NiAl) were embedded in the boiling liquid, under the sample and in the cylinder. The heat flux, temperature, superheat, and boiling heat transfer coefficient were related to the level of the microfins base. The heat flux was determined from the temperature gradient in the upper part of the heating cylinder, assuming one-dimensional heat conduction:

$$q = \frac{\lambda_{Cu} \cdot \pi d^2}{4A_{bs}} \cdot \frac{T_8 - T_5}{l_8 - l_5} \quad (1)$$

The extrapolated superheat, defined as the temperature difference between the reference surface and the saturated liquid, was as follows:

$$\Delta T = \frac{T_3 + T_4}{2} - q \left( \frac{l_{bs}}{\lambda_{Cu}} \right) - \frac{T_1 + T_2}{2} \quad (2)$$

According to Newton's law of cooling, for one-dimensional heat conduction, the heat transfer coefficient was defined as:

$$\alpha = \frac{q}{\Delta T} \quad (3)$$

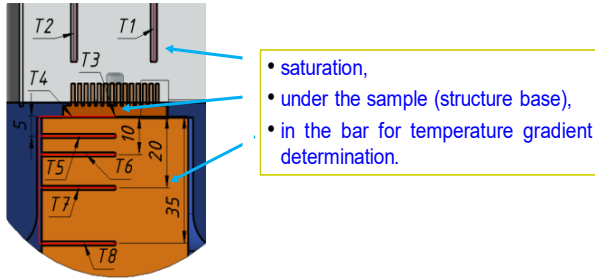


Fig. 6. Thermocouple arrangement.

### 3 Results

The following observations were drawn from the initial experiments (Figs. 7, 8):

- The highest values of the heat transfer coefficient (HTC) for boiling water (nearly 315 kW/m<sup>2</sup>K) were obtained for the sample with minichannels with additional microchannels (MMC) at a heat flux of about 1050 kW/m<sup>2</sup>. In the range of 600 – 1150 kW/m<sup>2</sup>, HTC was obtained above 250 kW/m<sup>2</sup>K.
- Approximately 30% higher heat transfer coefficient was obtained for the sample MMC compared to the best surface with minichannels (MC-0.8-6.0-2) using water and ethanol as working fluids.
- Compared to the plain smooth surface, the increase in HTC for the MMC surface was 6.6 times higher with a heat flux of about 500 kW/m<sup>2</sup> for boiling water.
- The MMC surface allowed to obtain significantly enlarged critical heat fluxes: approx. 1200 kW/m<sup>2</sup> with boiling water and approx. 1000 kW/m<sup>2</sup> with boiling ethanol.

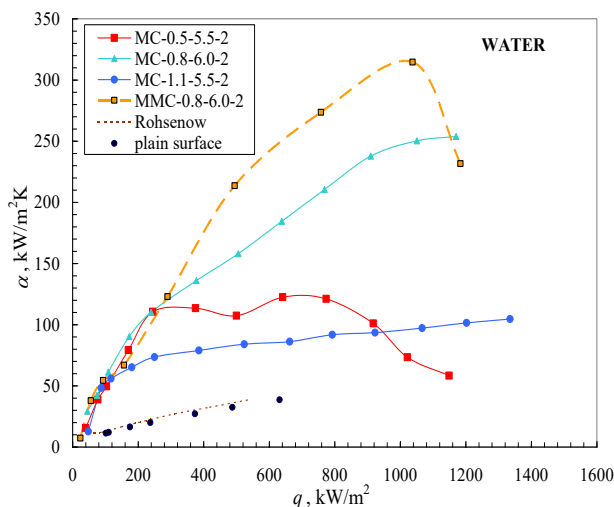


Fig. 7. Comparison of HTC for MC and MMC surfaces at boiling water.

The planned use of deeper microchannels cut with smaller pitches will contribute to increasing the density

of nucleation sites, which will result in the enlargement of the HTC.

When boiling water on flat surfaces with microchannels, the largest HTC was obtained at a depth of 0.4 – 0.5 mm [4,9], suggesting that the use of such cuts in the case of MMC surfaces will allow for a further increase in the heat transfer coefficient.

A preliminary visualization of the boiling of water on MC and MMC surfaces is shown in Figs. 9 and 10. The bubble formed at the bottom of the minichannel increases in volume and expands vertically, creating an elongated vapor plug. After the minifin tips are reached, a spherical vapor bubble is formed, which increases in volume at the expense of reduced vapor volume in the minichannel.

The first phase of bubble growth occurred between the minifins that border the minichannel. The second phase of growth occurred after the bubble moved to the top of the minifin.

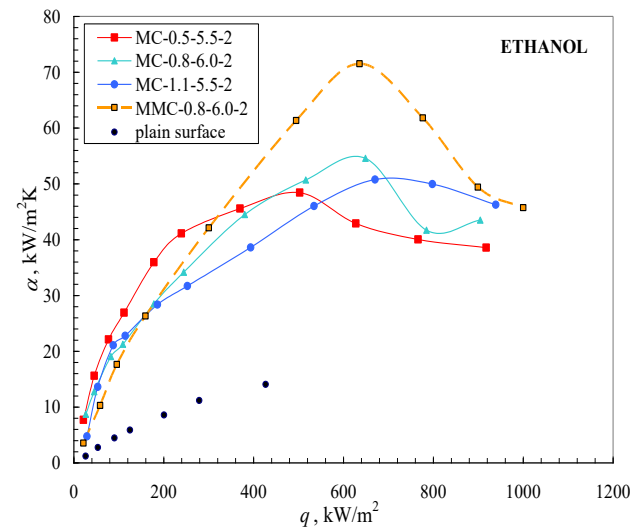


Fig. 8. Comparison of HTC for MC and MMC surfaces at boiling ethanol.

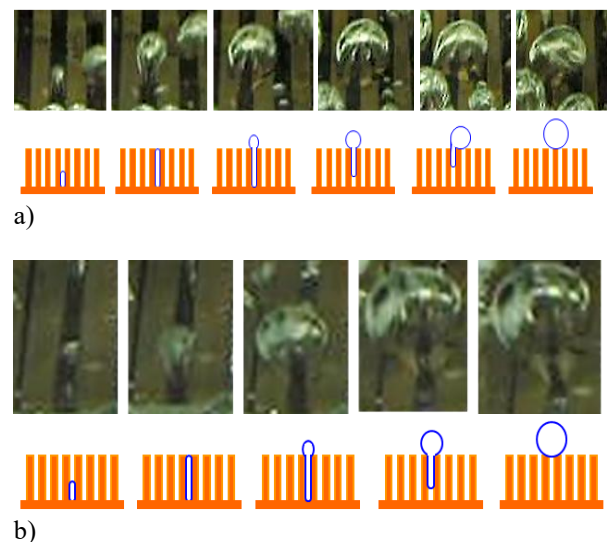
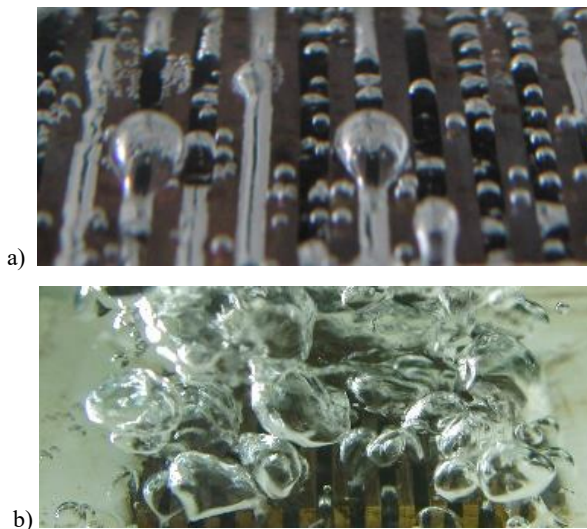


Fig. 9. Initial visualization: bubble formation for water pool boiling on the surface: a) MC-0.8-6.0-2.0,  $q \approx 43 \text{ kW/m}^2$ ,  $\Delta T = 1.6 \text{ K}$ , b) MC-0.5-5.5-2.0,  $q \approx 38 \text{ kW/m}^2$ ,  $\Delta T = 1.6 \text{ K}$ .



**Fig. 10.** Initial external visualization of water boiling; a) onset of nucleate boiling for sample MC-0.8-6.0-2, b) MMC-0.8-6.0-2,  $q = 91 \text{ kW/m}^2$ .

#### 4 Proposition of boiling models for MMC (assumptions)

For double extended surface with mini- and microchannels, two variants of the models may be used.

- *Variant A.* Macroconvection with separate liquid-vapor pathways, main assumptions (Fig. 11a):

The incoming liquid acts as an impinging jet and flows toward the nucleation site; bubbles nucleate in microchannels at the bottom of the minichannel, slide along the sidewalls, or sweep over a prescribed flow path on the channel surface; the bubbles move to the fin top before departing, then they depart from the fin top or upper parts of the channel sidewalls; the departing bubbles act as pumps bringing in fresh liquid; minichannels operate as liquid reservoirs; at higher heat fluxes, microchannels enable liquid supply through flow along the channels.

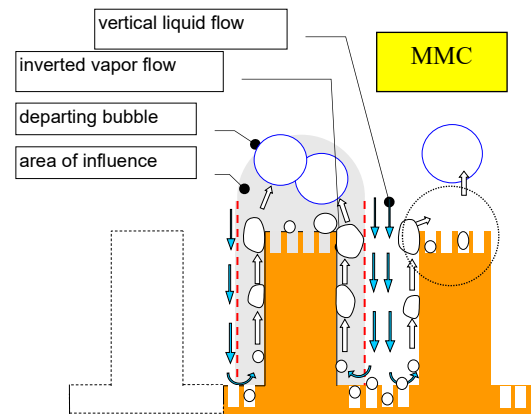
- *Variant B.* Suction-evaporation boiling mode:

This kind of boiling model was described by Pastuszko and Poniewski [17] for a double-extended surface in the form of connected horizontal and vertical subsurface tunnels. The mechanisms of liquid evaporation in tunnel corners and vapor bubbles cycle were accounted for, as well as the nonisothermality of the main fin, i.e., one-dimensional temperature distribution along vertical tunnel walls.

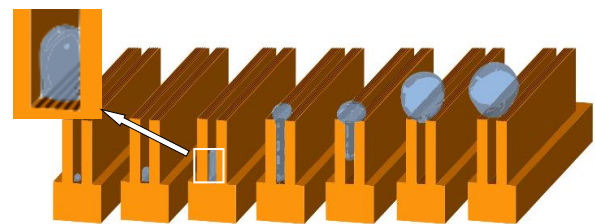
- *Variant C.* Complex boiling mode:

Figures 11a and 11b show the predicted boiling mechanism for the MMC surfaces. Microchannels will contribute to the onset of nucleate boiling (ONB) at low superheating, but at medium heat flux the heat transfer coefficient decreases after dry-out heat flux (DHF) is reached.

Minichannels improve pool boiling performance at higher heat flux: not only do they provide an additional surface for boiling heat transfer and nucleation, but they can prevent large bubbles from coalescing into a vapor blanket. This kind of vapor layer could cover the entire microchannel surface and ultimately dry out.



a)



b)

**Fig. 11.** Possible mechanisms of bubble generation in mini- and microchannels: a) separate liquid-vapor pathways, b) bubble growing.

Minichannels can eliminate this phenomenon, so that the critical heat flux (CHF) has higher values.

#### 5 Conclusions

This article presents a comparison of heat transfer coefficients during nucleate boiling for surfaces with minichannels and double extended surfaces, i.e., with minichannels and laser-etched microchannels. Preliminary results of visualization studies are presented and assumptions for the development of mechanistic models are provided.

The MMC surfaces increased critical heat flux (CHF) - up to approximately  $1200 \text{ kW/m}^2$  for water and  $1000 \text{ kW/m}^2$  for ethanol. The use of deeper microchannels with a lower pitch is expected to further enhance the nucleation site density and improve the HTC.

Boiling on MMC surfaces occurs in two stages: vapor bubbles form at the bottom of the minichannel, move upward, and transform into spherical bubbles at the fin tops. The minichannels prevent bubble coalescence into a vapor layer, reducing surface dry-out and enabling higher CHF values.

For minichannels 0.8 mm wide and 6 mm deep, additional surface texturization of the minichannels and minifin tips resulted in an approximately 30% increase in the maximum heat transfer coefficient for boiling both water and ethanol. The addition of microfins causes minor changes in the maximum heat flux. The assumptions presented for the formulation of theoretical models concern possible mechanisms of bubble generation in mini- and microchannels, i.e., separate liquid-vapor pathways and bubble growing phases.

## Nomenclature

$A$	– area, mm <sup>2</sup>
$a$	– aperture diameter, mm
$d$	– copper cylinder diameter, mm
HTC	– heat transfer coefficient, W/(m <sup>2</sup> K)
$h$	– depth, mm
$h_{fg}$	– enthalpy of vaporization, kJ/kg
$l$	– distance, mm,
MC	– minichannel,
MMC	– minichannel + microchannel
$p$	– pitch, mm,
$q$	– heat flux, kW/m <sup>2</sup> ,
$T$	– temperature, K,
$T1–T8$	– numbers of thermocouples
$w$	– width, mm

## Greek symbols

$\Delta T$	– temperature difference, K,
$\lambda$	– thermal conductivity, W/(mK)
$\delta$	– thickness, mm,
$\alpha$	– heat transfer coefficient, W/(m <sup>2</sup> K)

## Subscripts

$Cu$	– copper
$bs$	– base of specimen
$sat$	– saturation
$1$	– minichannel
$2$	– microchannel on minifin top
$3$	– microchannel on minichannel bottom

## References

1. S.G. Kandlikar, Enhanced macroconvection mechanism with separate liquid-vapor pathways to improve pool boiling performance. *J. Heat Transfer* **139**, 051501-051501-11 (2017) <https://doi.org/10.1115/1.4035247>
2. T.S.Emery, A.Jaikumar, P.Raghupathi, I.Joshi, S.G. Kandlikar, Dual enhancement in HTC and CHF for external tubular pool boiling – A mechanistic perspective and future directions. *Int. J. Heat Mass Transfer*, **122**, 1053-1073 (2018) <https://doi.org/10.1016/j.ijheatmasstransfer.2018.01.138>
3. Ł.J. Orman, Boiling heat transfer on meshed surfaces of different aperture, in in Proceedings of the Int. Conf. on Application of Experimental and Numerical Methods in Fluid Mechanics and Energetics, Liptovsky Jan, Slovakia, 9–11 April 2014, AIP Conference Proceedings 1608, 169-172 (2014) <https://doi.org/10.1063/1.4892728>
4. D. Cooke, S.G.Kandlikar, Pool boiling heat transfer and bubble dynamics over plain and enhanced microchannels. *J. Heat Transfer*, **133**, 052902-052909 (2011) <https://doi.org/10.1115/FEDSM-ICNMM2010-31147>
5. D. Cooke, S.G.Kandlikar, Effect of open microchannel geometry on pool boiling enhancement. *Int. J. Heat Mass Transfer*, **55**, 1004-1013 (2012) <https://doi.org/10.1016/j.ijheatmasstransfer.2011.10.010>
6. C.M. Patil, S.G. Kandlikar, Pool boiling enhancement through microporous coatings selectively electrodeposited on fin tops of open microchannels. *Int. J. Heat Mass Transfer*, **79**, 816-828 (2014) <https://doi.org/10.1016/j.ijheatmasstransfer.2014.08.063>
7. A.Kalani, S.G.Kandlikar, Pool boiling heat transfer over microchannel surfaces with ethanol at atmospheric pressure, in Proceedings of the ASME 10th Int. Conf. Nanochannels, Microchannels and Minichannels, Rio Grande, Puerto Rico (2012), 333-339
8. A.Jaikumar, S.G.Kandlikar, Enhanced pool boiling heat transfer mechanisms for selectively sintered open microchannels. *Int. J. Heat Mass Transfer*, **88**, 652–661(2015) <https://doi.org/10.1016/j.ijheatmasstransfer.2015.04.100>
9. A.M.Gheitaghy, A. Samimi, H. Saffari, Surface structuring with inclined minichannels for pool boiling improvement. *Appl. Therm. Eng.*, **126**, 892-902 (2017) <https://doi.org/10.1016/j.applthermaleng.2017.07.200>
10. R. Kaniowski R. Pastuszko R, Pool boiling of water on surfaces with open microchannels. *Energies*, **14**, 3062 (2021) <https://doi.org/10.3390/en14113062>
11. S. Hozejowska, R. Kaniowski, R. Pastuszko, Application of the trefftz method for pool boiling heat transfer on open microchannel surfaces. *Heat Transfer Eng.*, **43**, 362–370 (2022) <https://doi.org/10.1080/01457632.2021.1874669>
12. A. Kalani, S.G. Kandlikar, Enhanced pool boiling with ethanol at subatmospheric pressures for electronics cooling. *J. Heat Transfer*, **135**, 111002-111002-7 (2013) <https://doi.org/10.1115/1.4024595>
13. M.M. Rahman, M.McCarthy, Effect of Length Scales on the Boiling Enhancement of Structured Copper Surfaces. *J. Heat Transfer*, **139**, 111508-111508-9 (2017) <https://doi.org/10.1115/1.4036693>
14. H. J. Kwak, J.H. Kim, B. Myung, M.H. Kim, D.E. Kim, Behavior of pool boiling heat transfer and critical heat flux on high aspect-ratio microchannels. *Int. J. Thermal Sci.*, **125**, 111-120 (2018) <https://doi.org/10.1016/j.ijthermalsci.2017.11.025>
15. A.Walunj, A.Sathyabhama, Comparative study of pool boiling heat transfer from various microchannel geometries. *Appl. Therm. Eng.*, **128**, 672–683 (2018)

<https://doi.org/10.1016/j.applthermaleng.2017.08.157>

16. Ł.J.Orman, N.Radek, J.Pietraszek, J. Wojtkowiak, M. Szczepaniak, Laser Treatment of Surfaces for Pool Boiling Heat Transfer Enhancement. *Materials*, **16**, 1365 (2023)  
<https://doi.org/10.3390/ma16041365>
17. R.Pastuszko, M.E.Poniewski, Semi-analytical approach to boiling heat fluxes calculation in subsurface horizontal and vertical tunnels. *Int. J. Thermal Sci.*, **47**, 1169–1183 (2008)  
<https://doi.org/10.1016/j.ijthermalsci.2007.10.003>